Journal of Solid State Chemistry **152,** 453–459 (2000)
doi:10.1006/jssc.2000.8711, available online at http://www.idealibrary.com on IDEAL®

Structural and Luminescent Properties of a Nasicon-Type Phosphate $Cu^{I}_{0.5}Mn^{II}_{0.25}Zr_2(PO_4)_3$

A. Mouline,* M. Alami,* R. Brochu,† R. Olazcuaga,‡,[1] C. Parent,‡ and G. Le Flem‡

*Laboratoire de Chimie du Solide Appliquée—Laboratoire associé francophone L.A.F. 501, Faculté des Sciences, Avenue Ibn Batouta, BP 1014, Rabat, Marocco; †Laboratoire de Chimie du Solide et Inorganique Moléculaire (URA CNRS 1495), Groupe de Cristallochimie, Université de Rennes, Avenue du Général Leclerc, 35042 Rennes Cedex, France; and ‡Institut de Chimie de la Matière Condensée de Bordeaux, UPR CNRS 9048, 87, Avenue du Dr Albert Schweitzer, 33608 Pessac Cedex, France

Received December 7, 1999; in revised form February 16, 2000; accepted March 10, 2000

The phosphate $Cu^{I}_{0.5}Mn^{II}_{0.25}Zr_2(PO_4)_3$ can be obtained at 1000°C by exchange reaction in $Cu^{II}_{0.5}Zr_2(PO_4)_3$. It crystallizes in the rhombohedral system (space group $R\bar{3}$) with the parameters $a_h = 8.8352(1)$ Å and $c_h = 22.254(5)$ Å in the equivalent hexagonal cell. The structure refined by the Rietveld method is typical of Nasicon-type structure. Mn^{2+} ions occupy partially the M_1 site, while Cu^{+} ions are distributed over the M_1 and M_2 sites generated by the space group. This compound exhibits two fluorescences, occurring in the violet and orange regions and assigned respectively to isolated Cu^{+} and Mn^{2+} ions. Two other luminescences detected in the blue and green range at low temperature correspond respectively to $(Cu_2)^{+}$ and $(Cu^{+})_2$ pairs. Efficient energy transfer $Cu^{+} \rightarrow Mn^{2+}$ is observed at room temperature strengthening the orange emission of Mn^{2+} in the M_1 site. © 2000 Academic Press

INTRODUCTION

3*d*-transition element ions can be easily introduced in Nasicon-type phosphates and related structures (1–5) which have the general composition $M(1)_nM(2)_mX_2(PO_4)_3$, where $M(1)$ and $M(2)$ characterize the sites created by the covalent framework $X_2(PO_4)_3$, X being mostly Ti or Zr. The existence of vacancies in the skeleton involves structure types such as $NaZr_2(PO_4)_3$ or $\beta Fe_2(SO_4)_3$ (6,7). Such $X_2(PO_4)_3$ skeletons allow the induction of redox reactions without alteration of the crystal structure. The redox system $Cu^{2+} + e^{-} \Leftrightarrow Cu^{+}$ was discovered to occur in the thermal evolution of $Cu^{I}(Ti, Zr)_2(PO_4)_3$ (1,8) and reported later for $Cu^{I}Hf_2(PO_4)_3$ (9). Ultimately copper whiskers were anchored in $X_2(PO_4)_3$ (10) and nucleation of Ag° was evidenced on $AgZr_2(PO_4)_3$ (11). Proton exchange was also mentioned in the reaction $4Cu^{II}_{0.5}Zr_2(PO_4)_3 + H_2 \rightarrow 4H_{0.5}Cu^{I}_{0.5}Zr_2(PO_4)_3$. The copper(II) phosphate can be restored under a stream of oxygen (8, 12).

Such reactions were tentatively applied in the domain of the heterogeneous catalysis. New catalysts were synthesized by inducing supported metal particles and can give rise to periodic reactions (13).

In this context the object of this publication is to demonstrate the possibility of such exchange reactions to the preparation of new compounds. A new phase $Cu^{I}_{0.5}Mn^{II}_{0.25}Zr_2(PO_4)_3$ will be described from the structural viewpoint, and its luminescent properties will be discussed in relation to the manganese copper ions distribution.

COMPOUND PREPARATION

The phosphate $Cu^{I}_{0.5}Mn^{II}_{0.25}Zr_2(PO_4)_3$ was obtained by reducing $Cu^{II}_{0.5}Zr_2(PO_4)_3$ by the manganese as metal according to the schematic reaction:

$$Cu^{II}_{0.5}Zr_2(PO_4)_3 + 0.25Mn \rightarrow Cu^{I}_{0.5}Mn^{II}_{0.25}Zr_2(PO_4)_3.$$

$Cu^{II}_{0.5}Zr_2(PO_4)_3$ was prepared through a sol–gel route previously described (14), and the reaction with the metallic Mn was carried out in a sealed quartz tube under vacuum. Actually this reaction occurs in two steps identified by X-ray diffraction.

(i) at 700°C a partial manganese/copper exchange is observed corresponding to the intermediate process:

$$Cu^{II}_{0.5}Zr_2(PO_4)_3 + 0.25Mn \rightarrow$$
$$Cu^{II}_{0.5}Mn^{II}_{0.25}Zr_2(PO_4)_3 + 0.25Cu$$

(ii) at 1000°C the copper metal reduces the remaining cupric ions according to the reaction:

$$Cu^{II}_{0.5}Mn^{II}_{0.25}Zr_2(PO_4)_3 + 0.25Cu$$
$$\rightarrow Cu^{I}_{0.5}Mn^{II}_{0.25}Zr_2(PO_4)_3$$

The obtained powder is white.

[1] To whom correspondence should be addressed. E-mail: olaz@icmcb.u-bordeaux.fr.

0022-4596/00 $35.00

The chemical analysis of the final product agrees with the expected formula.

Incidentally the thermal variation of the reciprocal molar magnetic susceptibility between 4 and 300 K is linear. The experimental Curie constant ($C = 1.07$ emu K/mol) is consistent with the calculated value ($C = 1.09$ emu K/mol) assuming the only contribution of the 0.25 Mn^{2+}. Nevertheless, EPR experiments indicate the existence of small Cu^{2+} proportion.

STRUCTURAL INVESTIGATION

The XRD pattern can be indexed assuming a rhombohedral cell. The order of magnitude of the parameters in the equivalent hexagonal (h) cell, $a_h = 8.8352 \pm 0.0001$ Å, $c_h = 22.254 \pm 0.005$ Å, is typical of a Nasicon-type structure. The densities ($d_{exp.} = 3.38$ g/cm^3, $d_{calc.} = 3.40$ g/cm^3) imply six $Cu^{I}_{0.5}Mn^{II}_{0.25}Zr_2(PO_4)_3$ formulae per unit cell.

The indexation of all reflections agrees with the $R\bar{3}$ or $R32$ space groups (Table 1).

The refinement of the structure was carried out using the Rietveld profilation method.

The X-ray diffraction data were collected at room temperature with a diffractometer using a graphite monochromator. The conditions used for the data collection are given in the Table 2.

TABLE 1
Powder Diffraction Data of $Cu^{I}_{0.5}Mn^{II}_{0.25}Zr_2(PO_4)_3$

$h\ k\ l$	d_{obs} (Å)	d_{calc} (Å)	I/I_0
003	7.39	7.41	3
012	6.309	6.305	15
104	4.504	4.499	65
110	4.419	4.418	100
113	3.798	3.795	90
202	3.616	3.618	3
024	3.155	3.152	55
211	2.869	2.868	15
116	2.843	2.841	60
018	2.616	2.614	8
214	2.568	2.566	28
300	2.551	2.551	30
208	2.251	2.249	8
220	2.209	2.208	3
119	2.158	2.158	5
217	2.140	2.139	5
10 10	2.136	2.135	5
223	2.116	2.117	5
306	2.102	2.102	5
128	2.006	2.005	15
134	1.984	1.983	12
02 10	1.924	1.923	8
226	1.899	1.898	14
00 12	1.857	1.855	3
404	1.811	1.812	5
309	1.769	1.765	13
318	1.692	1.687	10
324	1.675	1.674	20

TABLE 2
Conditions Used for Data Collection of X-Ray Diffraction

Sample container	Inox
Diffractometer	Philips PW 3040/00
Monochromator	Graphite
Instrument geometry	Bragg–Brentano θ–θ
Wavelength (Å)	1.5418
Data collection range, 2θ (°)	10–120
2θ step (°), counting time (s)	0.02, 30
Refinement program	Fullprof[a]
Background	Points file
Absorption correction	No
Preferred orientation	No
Law for full-width at half maximum (FWHM)	$(FWHM)^2 = U\tan^2\theta + V\tan\theta + W$ $U = 0.109$, $V = 0.0022$, $W = 0.011$
Analytical function for profile shape	Pseudo-Voigt (PV) $PV = \eta L + (1-\eta)G$, $\eta = 0.29$
a_h (Å)	8.8352(1)
c_h (Å)	22.254(5)
Space group	$R\bar{3}$
Number of reflections	514
R_p	0.13
R_{wp}	0.15
R_B	0.04
R_F	0.03
χ^2	1.9

[a] J. Rodriguez-Carvajal, Powder Diffraction Satellite Meeting of the XVth Congress of IUCR, Toulouse, 1990. Abstract, p. 127.

Calculations were made assuming the $R\bar{3}$ space group and the initial atomic coordinates were equivalent to those of $Cu^{I}Zr_2(PO_4)_3$ in the $R\bar{3}c$ (2) space group. This symmetry lowering results from the splitting of the general (36f) x, y, z positions into two (18f) positions. Final satisfactory refinement factors were obtained as the manganese atoms were introduced in half of the usually labeled $M(1)$ sites of the Nasicon structure, and the copper was distributed over the remaining $M(1)$ and $M(2)$ sites with respective rates of 85% and 15%. In addition, the copper atoms in the $M(1)$ oxygenated antiprism were delocalized with a statistical occupancy of $\frac{1}{6}$ in the same configuration previously reported for $Cu^{I}Zr_2(PO_4)_3$ (2). The tentative introduction of copper in only one of these sites results in non realistic large isotropic thermal parameters. The resulting atomic coordinates and their esd's are listed in Table 3. A comparison between the experimental and calculated X-ray diffraction data is presented in Fig. 1. Table 4 collects selected bonds and distances.

From a structural point of view the structure of $Cu^{I}_{0.5}Mn^{II}_{0.25}Zr_2(PO_4)_3$ can be considered as a "mixture" of the structural arrangements of $Cu^{I}Zr_2(PO_4)_3$ (2) and $Mn_{0.5}Zr_2(PO_4)_3$ (4) (Fig. 2). The skeleton "$Zr_2(PO_4)_3$" is preserved and consists of PO_4 tetrahedra sharing corners with ZrO_6 octahedra in a three-dimensional network. The

TABLE 3
Final Positional and Thermal Parameters and Occupancy Factors of $Cu^{I}_{0.5}Mn^{II}_{0.25}Zr_2(PO_4)_3$

Atom	Site	x	y	z	B_{iso} (Å)^2	Occupancy
Mn	3(a)	0	0	0.5	1.20(2)	0.5
Cu_1	18(f)	−0.038(1)	−0.137(1)	−0.004(1)	2.36(4)	0.142
Cu_2	18(f)	0.319(1)	0.152(1)	0.366(1)	1.98(4)	0.025
Zr_1	6(c)	0	0	0.141(1)	0.21(2)	1
Zr_2	6(c)	0	0	0.645(2)	0.21(2)	1
P	18(f)	0.282(1)	−0.011(1)	0.248(1)	0.64(3)	1
O_1	18(f)	0.205(1)	0.175(1)	0.086(1)	1.02(4)	1
O_{11}	18(f)	0.160(1)	0.179(1)	0.419(1)	1.02(4)	1
O_2	18(f)	0.172(1)	−0.037(1)	0.192(1)	1.02(4)	1
O_{22}	18(f)	0.009(1)	0.193(1)	0.303(1)	1.02(4)	1

PO_4 tetrahedra are slightly distorted, $\Delta_{P-O} = 0.09$ Å, in comparison with the values reported for the copper or the manganese phosphates, $\Delta_{P-O} = 0.04$ Å. In contrast, both ZrO_6 octahedra are almost regular. The Mn–O distance in the $M(1)$ antiprism, 2.35 Å, is close to the distance found in the pure manganese phosphate, 2.31 Å.

In oxides the usual environment of Cu^{I} is linear (Cu_2O, delafossite, etc.). This dumbbell-like geometry is characterized by Cu^{I}–O distances included between 1.79 and 1.90 Å (15–17). Decreasing the O–Cu^{I}–O angle leads to an increase of the Cu^{I}–O distances. For instance, in tetrahedral coordination the Cu^{I}–O distances range from 2.08 to 2.25 Å (18, 19). The copper (Cu^{I}) environment, located in the $M(1)$ antiprism, reproduces exactly the structural configuration reported for $Cu^{I}M_2(PO_4)_3$ (M = Ti, Zr) (1, 2): displacement from the center of the site in six possible positions and creation of two short Cu^{I}–O distances at 2.10 and 2.26 Å. In addition the coexistence of two Cu atoms within the same antiprism was demonstrated for $Cu^{I}Zr_2(PO_4)_3$ with a Cu^{I}–Cu^{I} distance 2.25 Å. In the investigated phosphate the largest Cu^{I}–Cu^{I} distance in $M(1)$ is 2.18 Å. The existence of such pairs will be discussed later with respect to the luminescent properties.

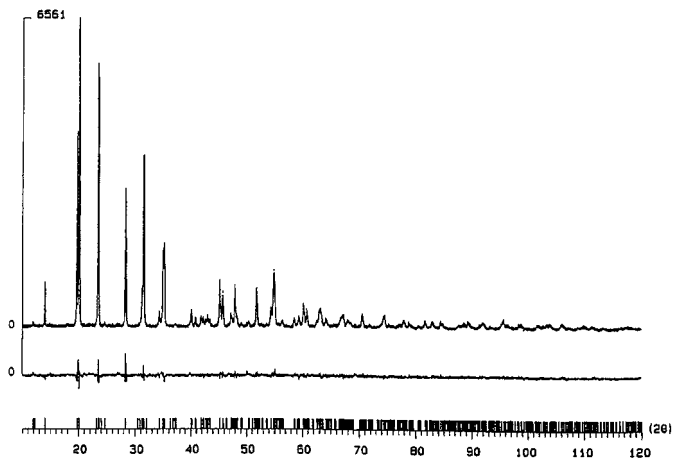

FIG. 1. Comparison between the experimental and calculated X-ray diffraction data.

In the large $M(2)$ sites, assuming Cu^{I}–O distances lower than 3 Å, the copper is surrounded by five oxygens and more specifically by three oxygens at short distances, respectively Cu_2–O_{11} = 1.92 Å, Cu_2–O_{22} = 1.94 Å, and Cu_2–O_1 = 2.08 Å. Actually the copper is located approximately at the middle of the hypotenuse of a right-angled triangle limited by O_{11}, O_{22}, and O_1 with the angle $\approx 90°$. This triangle shares a common edge with the Zr_2O_6 octahedron and with a PO_4 tetrahedron (Zr_2–P = 3.41 Å). Moreover, the shortest Cu_1–Cu_2 distance compatible with the creation of a copper–copper bond is 2.23 Å, which is close to the largest Cu_1–Cu_1 distance within $M(1)$ and nearly the same value than the Cu^{I}–Cu^{I} pairs evidenced in $Cu^{I}Zr_2(PO_4)_3$. Therefore a close examination of a connection between the $M(1)$ and $M(2)$ sites leads to consider the possible formation of a quasi-linear copper tetramer involving Cu_1 and Cu_2 in a cavity limited by two Zr_1O_6 and two Zr_2O_6 octahedra and two PO_4 tetrahedra where the copper–copper distances are quasi-constant and successively 2.23, 2.18, and 2.23 Å (Fig. 3). Obviously such a cluster can be reduced to dimer or trimer, the tetramer being the limiting case consistent with the volume of the cavity but not consistent with the composition at the macroscopic scale since the number of copper in the unit cell is 3. The formation of such clusters was theoretically explained by the calculation of MEHOTRA and HOFMANN (20). The hybridized valence orbitals, by introducing an s and p character in the d function of d^{10} cations, can be constructed with a weak but real attractive interaction.

LUMINESCENT PROPERTIES

Excitation and emission spectra have been recorded at 5, 85, and 300 K using a SPEX FL 212 fluorimeter equipped with a SMC liquid helium cryostat. The excitation source was a high-pressure xenon lamp emitting between 200 and 1000 nm.

The emission spectrum recorded at 300 K is given in Fig. 4. A single broadband with a maximum occurring at about 580 nm can be observed under an extended excitation range (250 nm $< \lambda_{exc} <$ 500 nm). An additional small peak can be detected in the high-energy side of the broad band peaking between 410 and 430 nm and a shoulder located at about 415 nm (Fig. 4-insert). The excitation spectra were recorded for three emission wavelengths: 425, 580, and 650 nm. The excitation spectrum of the 425 nm emission exhibits a broadband that can be divided into two main components peaking at 264 and 285 nm with a shoulder located at about 315 nm. For the two other wavelengths, the same bands are observed and additional lines typical of

TABLE 4
Selected Bond Lengths (Å) and Angles (Deg) for $Cu^{I}_{0.5}Mn^{II}_{0.25}Zr_2(PO_4)_3$

Zr_1–O_1	2.08(2)	O_1–P–O_2	113(2)	Cu_1–Cu_1	2.18(3)
Zr_1–O_2	2.05(2)	O_1–P–O_{11}	107(2)	O_1–Cu_1–O_1	133(4)
O_1–Zr_1–O_1	89.5(15)	O_1–P–O_{22}	108(2)	Cu_2–O_1	2.08(4)
O_1–Zr_1–O_2	90.1(13)	O_2–P–O_{22}	109(2)	Cu_2–O_1	3.14(2)
O_1–Zr_1–O_2	92.2(15)	O_{11}–P–O_2	104(2)	Cu_2–O_1	2.92(1)
Zr_2–O_{11}	2.07(1)	O_{11}–P–O_{22}	112(2)	Cu_2–O_{11}	1.92(2)
Zr_2–O_{22}	2.03(2)	Mn–O_{11}	2.35(1)	Cu_2–O_{11}	2.95(2)
O_{11}–Zr_2–O_{11}	77.9(13)	O_{11}–Mn–O_{11}	67.3(10)	Cu_2–O_{22}	3.25(2)
O_{11}–Zr_2–O_{22}	91.5(13)	Cu_1–O_1	3.21(3)	Cu_2–O_{22}	1.94(1)
O_{22}–Zr_2–O_{22}	90.57(13)	Cu_1–O_1	3.08(5)	Cu_2–O_{22}	2.82(1)
P–O_1	1.54(2)	Cu_1–O_1	2.10(4)	O_1–Cu_2–O_{11}	121(9)
P–O_{11}	1.59(2)	Cu_1–O_1	2.26(5)	O_1–Cu_2–O_{22}	114(8)
P–O_2	1.53(2)	Cu_1–O_1	2.44(5)	O_{11}–Cu_2–O_{22}	120(7)
P–O_{22}	1.50(2)	Cu_1–O_1	3.32(3)	Cu_1–Cu_2	2.23(4)

Mn^{2+} can be detected between 400 and 550 nm by increasing the magnification of the recording (Fig. 5 and insert).

At 85 K under a 260 nm excitation, the violet emission ($\lambda_{em} = 410$ nm) is clearly isolated from the orange emission which can be also recorded with a 320 nm excitation (Fig. 6).

Finally at very low temperature (5 K) the violet and orange emissions persist ($\lambda_{exc} = 260$ nm), but the intensity of the latter decreases strongly. Moreover, a broad shoulder is observed on the high-energy side which can be decomposed in two bands peaking at approximately 460 and 540 nm (Fig. 7). The corresponding excitation spectra are given in Fig. 8. The blue and green emissions exhibit a single band with a maximum occurring at about 305 nm, whereas the excitation spectrum of the orange emission is characterized by the two intense bands located at 260 and 285 nm in addition to the features corresponding to the Mn^{2+} ions observed around 400–500 nm. Actually the excitation band at 260 nm corresponds to the violet emission. These experimental facts are summarized in the Table 5.

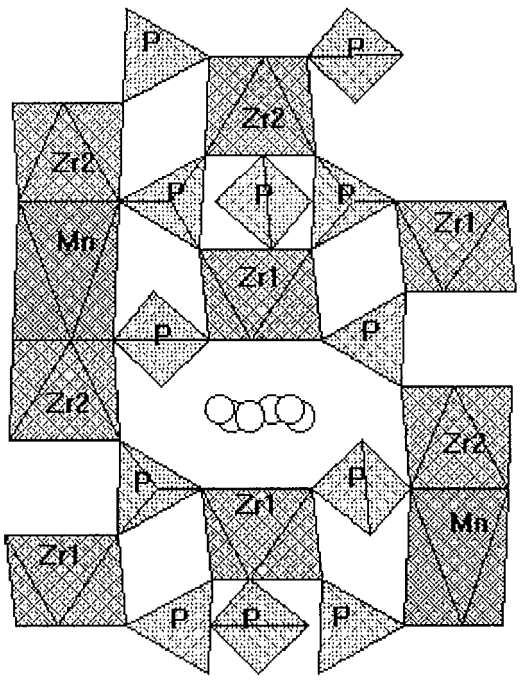

FIG. 2. Part of the ⟨110⟩ projection of the structure of $Cu^{I}_{0.5}Mn^{II}_{0.25}Zr_2(PO_4)_3$ illustrating the location of the Cu_1 (○) and Mn sites in the $Zr_2(PO_4)_3$ skeleton.

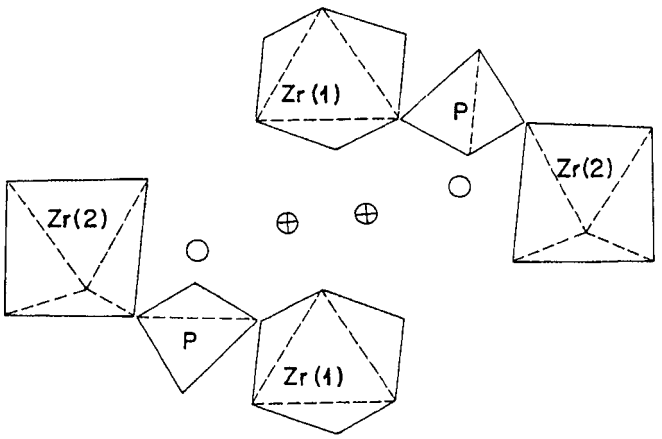

FIG. 3. Hypothetical quasi-linear Cu_2–Cu_1–Cu_1–Cu_2 tetramer in the cavity limited by the Zr_1O_6, Zr_2O_6 octahedra and the PO_4 tetrahedron at the connection between the Cu_1 (⊕) and the Cu_2 sites (○).

DISCUSSION

The interpretation of these luminescence spectra needs to briefly report the previous data related to the luminescent properties of $Mn_{0.5}Zr_2(PO_4)_3$ and $Cu^{I}Zr_2(PO_4)_3$ (4, 21).

The Mn^{2+} ions in the manganese phosphate are located in two anti-prismatic sites with Mn–O distances of

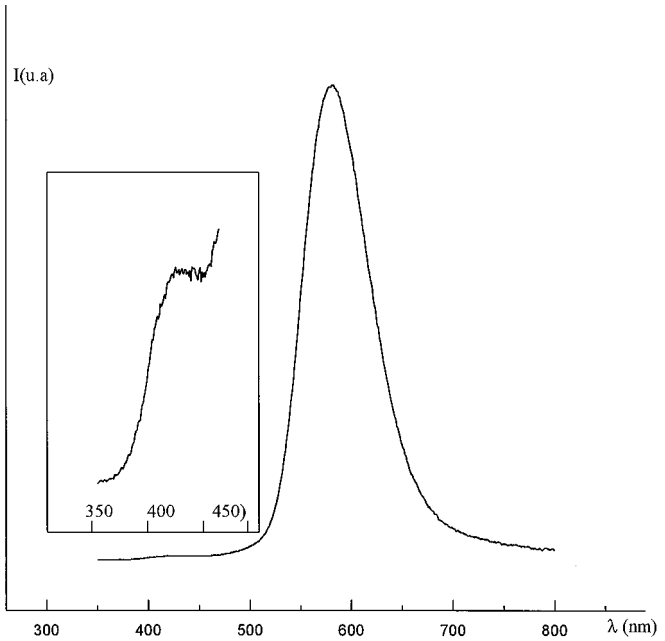

FIG. 4. Emission spectrum of $Cu^{I}_{0.5}Mn^{II}_{0.25}Zr_2(PO_4)_3$ under 260 nm excitation. (Insert) High component after magnification of the emission spectrum between 400 and 450 nm ($T = 300$ K).

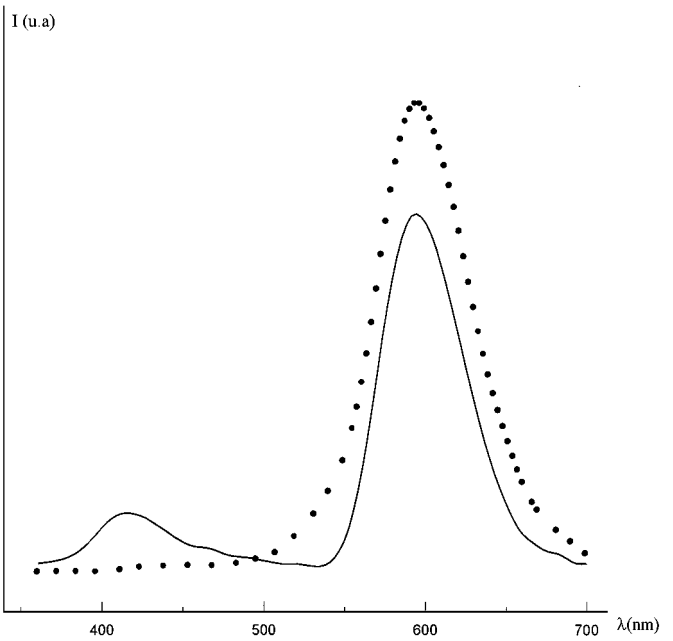

FIG. 6. Emission spectrum of $Cu^{I}_{0.5}Mn^{II}_{0.25}Zr_2(PO_4)_3$ ($T = 85$ K; —, $\lambda_{exc} = 260$ nm; ●, $\lambda_{exc} = 320$ nm).

respectively 2.31 and 2.54 Å. This last value is overestimated since this distance reflects a partial occupation of the antiprismatic sites. These manganese centers give rise to two emission bands located respectively at 570 and 610 nm and typical excitation spectra with several lines appearing between 340 and 485 nm.

The copper phosphate exhibits two fluorescences occurring in the violet ($\lambda_{em} \approx 410$ nm) and green ($\lambda_{em} \approx 550$ nm). They are assigned to two different centers: the violet one to

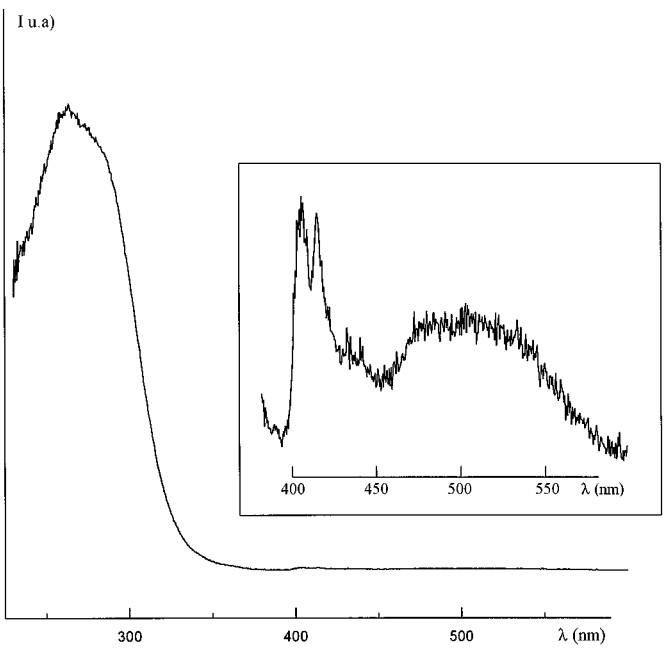

FIG. 5. Excitation spectrum of $Cu^{I}_{0.5}Mn^{II}_{0.25}Zr_2(PO_4)_3$ ($\lambda_{em} = 650$ nm, $T = 300$ K). (Insert) Magnification of the spectrum between 400 and 550 nm.

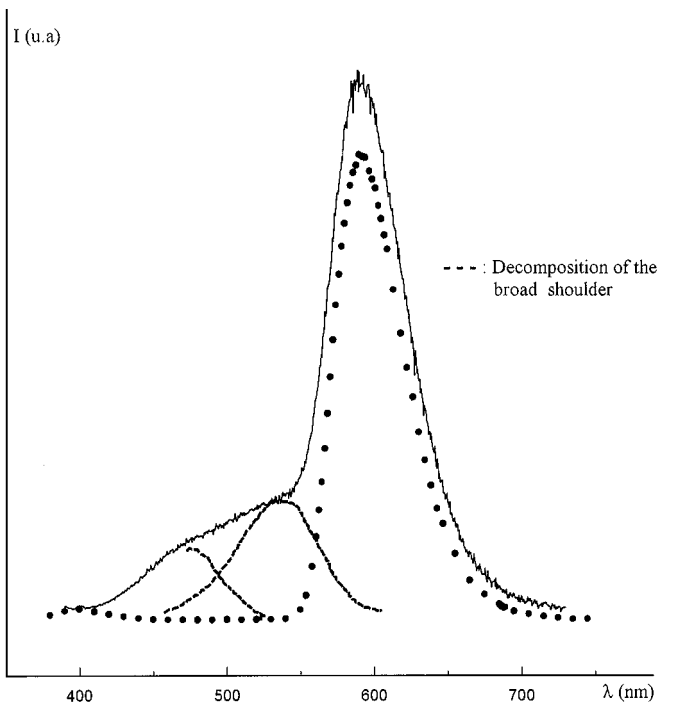

FIG. 7. Emission spectrum of $Cu^{I}_{0.5}Mn^{II}_{0.25}Zr_2(PO_4)_3$ ($T = 5$ K; ●, $\lambda_{exc} = 260$ nm; —, $\lambda_{exc} = 320$ nm).

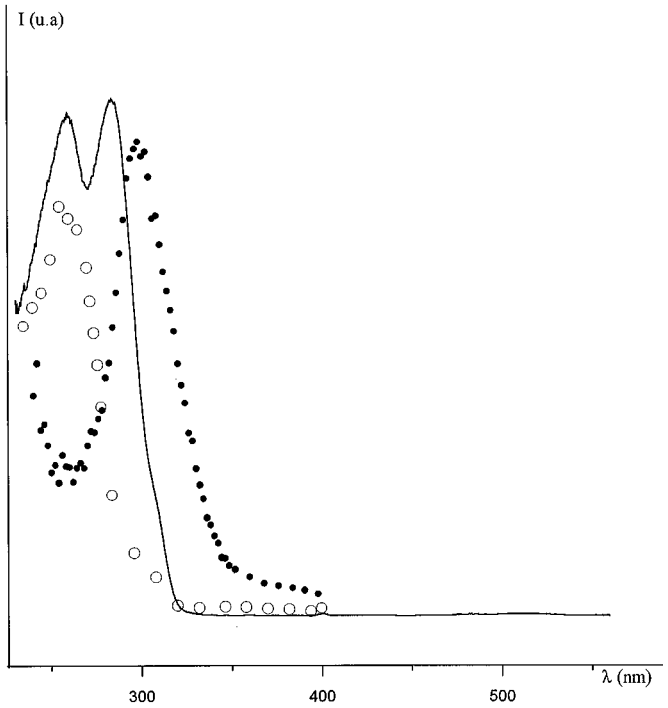

FIG. 8. Excitation spectrum of $Cu^{I}_{0.5}Mn^{II}_{0.25}Zr_2(PO_4)_3$ ($T = 5$ K; —, $\lambda_{em} = 580$ nm; ○, $\lambda_{em} = 410$ nm; ●, $\lambda_{em} = 460$ or 540 nm).

isolated Cu^+ and the green one to Cu^+–Cu^+ pairs occupying the same sites. These results were in agreement with structural investigations using X-ray, neutron, and EXAFS measurements (2, 22). An additional blue fluorescence was observed at $\lambda = 460$ nm and was tentatively attributed to Cu_2^+ pairs due to its very fast lifetime (≈ 20 ns). The excitation spectrum of the violet emission exhibits a single band peaking at 265 nm at 6.5 K, and the green fluorescence comprises two distinct bands centered at 250 and 310 nm. Moreover, a large overlap is observed between the violet and the blue excitation spectra. Finally, it is important to mention the exact matching between the isolated copper emission and the position of the $^6A_1 \rightarrow {}^4A_1{}^4E(^4G)$ excitation band of Mn^{2+} in these phosphates at about 400 nm.

From these data the orange emission can be attributed to the Mn^{2+} center with probably, at 85 and 300 K, a contribution of Cu^+–Cu^+ pairs. This attribution is consistent with the Mn–O distance of 2.35 Å. The violet emission can be assigned to isolated Cu^+ and the blue and green ones to $(Cu_2)^+$ and Cu^+–Cu^+ pairs, respectively. In agreement with the last remark of the previous paragraph, a $Cu^+ \rightarrow Mn^{2+}$ energy transfer is clearly demonstrated by the appearance of copper bands in the Mn^{2+} excitation spectra of the orange emission (Fig. 8). The green emission that prevails in $Cu^{I}Zr_2(PO_4)_3$ is detected in the investigated phosphate only at low temperature with a small intensity by the strong reduction of the orange band width which occurs between 85 and 5 K. Actually the number of copper pairs and/or extended cluster cannot be estimated in the copper manganese phase but they exist probably in small proportion.

Lastly the probability of formation of $(Cu_2)^+$ centers must be discussed. Such copper(I) phosphates are sensitive to oxidation, and small quantities of Cu^{2+} ions were revealed unambiguously by ESR measurements. During the oxidation, an electron transfer may occur between two close Cu^+ and $(Cu^+)_2$ centers giving rise to $(Cu_2)^+$ centers according to the following oxido-reduction process: $Cu^+ \rightarrow Cu^{2+} + e^-$ and $(Cu^+)_2 + e^- \rightarrow (Cu_2)^+$. $(Cu_2)^+$ can be considered to be a Cu^+–Cu^0 pair.

CONCLUSION

The new phosphate $Cu^{I}_{0.5}Mn^{II}_{0.25}Zr_2(PO_4)_3$ is the first example of simultaneous introduction of copper(I) and manganese(II) in Nasicon-type phosphate thanks to exchange reaction. The location of metallic ions within the $Zr_2(PO_4)_3$ framework reproduces the cation distribution previously reported for the pure manganese(II) and copper(I) phosphates (2, 4). The proportion of copper in the two different sites is obviously dependent on the elaboration conditions but reflects also the stabilization of copper(I) aggregates previously observed in solid state as well in coordination compounds (23).

TABLE 5
Location of the Emission and Excitation Bands for $Cu^{I}_{0.5}Mn_{0.25}Zr_2(PO_4)_3$

		Wavelength	
Temperature	Attribution (see discussion)	Emission maxima (nm)	Excitation maxima (nm)
300 K	Cu^+	425	← 261, 285
	Mn^{2+}, $(Cu^+)_2$	580	← 264, 285, ≈ 400–500
85 K	Cu^+	410	← 260
	Mn^{2+}, $(Cu^+)_2$	580	← 264, 285, ≈ 400–500
5 K	Cu^+	410	← 260
	$(Cu_2)^+$, $(Cu^+)_2$	460, 540	← 305
	Mn^{2+}	580	← 264, 285, ≈ 400–500

The luminescent properties are strongly influenced by the exact overlapping of the isolated Cu^+ emission and Mn^{2+} high-intensity excitation band at $\lambda = 405$ nm. It results an efficient $Cu^+ \rightarrow Mn^{2+}$ energy transfer, which allows the particular copper emission to be observed only at low temperature. The formation of (Cu_2^+) center is made possible by the short interatomic distances within the copper clusters.

REFERENCES

1. A. Mbandza, E. Bordes, P. Courtine, A. El Jazouli, J. L. Soubeyroux, G. Le Flem, and P. Hagenmuller, *React. Solids* **5,** 315 (1988).
2. I. Bussereau, M. S. Belkhiria, P. Gravereau, A. Boireau, J. L. Soubeyroux, R. Olazcuaga, and G. Le Flem, *Acta Crystallogr. B* **48,** 1741 (1992).
3. H. Fakrane, A. Aatiq, M. Lamire, A. El Jazouli, and C. Delmas, *Ann. Chim.-Sci. Mater.* **23**(1–2), 81 (1988).
4. A. Mouline, R. Brochu, M. Alami, R. Olazcuaga, C. Parent, and G. Le Flem, *Mater. Res. Bull.* in press.
5. A. Jouanneaux, A. Verbaere, Y. Piffard, A. N. Fitch, and M. Kinoshita, *Eur. J. Solid State Inorg. Chem.* **28,** 683 (1991).
6. L. O. Hagman and P. Kierkegaard, *Acta Chem. Scand.* **22,** 1822 (1968).
7. P. C. Christidis and P. J. Rentzeperis, *Z. Kristallogr.* **141,** 233 (1975).
8. G. Le Pollés, A. El Jazouli, R. Olazcuaga, J. M. Dance, G. Le Flem, and P. Hagenmuller, *Mater. Res. Bull.* **22,** 117 (1987).
9. R. Ahmamouch, S. Arsalane, M. Kacimi, and M. Ziyad, *Mater. Res. Bull.* **32,** 755 (1997).
10. A. Mbandza, E. Bordes, and P. Courtine, *Mater. Res. Bull.* **20,** 251 (1985).
11. S. Arsalane, K. O. Hajali, M. Kacimi, R. Brochu, and M. Ziyad, *J. Chim. Phys.* **92,** 1428 (1995).
12. A. Serghini, M. Kacimi, M. Ziyad, and R. Brochu, *J. Chem. Phys.* **85,** 499 (1988).
13. R. Brochu, A. Lamzibri, A. Aadane, S. Arsalane, and M. Ziyad, *Eur. J. Solid State Inorg. Chem.* **28,** 253 (1991).
14. I. Bussereau, R. Olazcuaga, G. Le Flem, and P. Hagenmuller, *Eur. J. Solid State Inorg. Chem.* **26,** 383 (1989).
15. W. G. Wyckoff, "Crystal Structures", Vol. 1, 2nd ed. Inter Science Publishers, New York, 1965.
16. J. P. Doumerc, A. Ammar, A. Wichainchai, M. Pouchard, and P. Hagenmuller, *J. Phys. Chem. Solids* **48**(1), 37 (1987).
17. M. Louër, S. Arsalane, R. Brochu, M. Ziyad, and D. Louër, *Acta Crystallogr. B* **51,** 908 (1995).
18. B. O. Marinder, P. E. Werner, E. Walhstrom, and J. G. Malmros, *Acta Chem. Scand., Ser. A* **34,** 51 (1980).
19. E. M. Mc Carron III and J. C. Calabrese, *J. Solid State Chem.* **65,** 215 (1986).
20. P. K. Mehotra and R. Hoffman, *Inorg. Chem.* **17,** 2187 (1978).
21. P. Boutinaud, C. Parent, G. Le Flem, C. Pedrini, and B. Moine, *J. Phys.: Condens. Matter* **4**(E29), 3031 (1992).
22. E. Fargin, I. Bussereau, G. Le Flem, R. Olazcuaga, C. Cartier, and H. Dexpert, *Eur. J. Solid State Chem.* **29,** 975 (1992).
23. G. Le Flem, *J. Alloys Compounds* **188,** 36 (1992).